

Bright Solitary Waves on a Torus: Existence, Stability and Dynamics for the Nonlinear Schrödinger Model

J. D'Ambroise,¹ P.G. Kevrekidis,² and P. Schmelcher^{3,4}

¹ *Department of Mathematics, Computer & Information Science,
State University of New York (SUNY) College at Old Westbury, Westbury, NY, 11568, USA*

² *Department of Mathematics and Statistics, University of Massachusetts, Amherst, MA, 01003, USA*

³ *Center for Optical Quantum Technologies, Department of Physics,
University of Hamburg, Luruper Chaussee 149, 22761 Hamburg Germany*

⁴ *The Hamburg Centre for Ultrafast Imaging, University of Hamburg,
Luruper Chaussee 149, 22761 Hamburg, Germany*

Motivated by recent developments in the realm of matter waves, we explore the potential of creating solitary waves on the surface of a torus. This is an intriguing perspective due to the role of curvature in the shape and dynamics of the coherent structures. We find different families of bright solitary waves for attractive nonlinearities including ones localized in both angular directions, as well as waves localized in one direction and homogeneous in the other. The waves localized in both angular directions have also been partitioned into two types: those whose magnitude decays to zero and those who do not. The stability properties of the waves are examined and one family is found to be spectrally stable while most are spectrally unstable, a feature that we comment on. Finally, the nature of the ensuing nonlinear dynamics is touched upon.

PACS numbers:

I. INTRODUCTION

The atomic physics platform of Bose-Einstein condensates (BECs) has served over the past two decades as an excellent testbed for ideas stemming from nonlinear waves and their interplay with geometric and topological notions among many others [1–3]. In particular, a wide variety of experiments has been performed to explore ideas related to bright coherent structures in effectively self-focusing and attractively interacting BECs [4–7] and related to repulsively interacting BECs with their effective self-defocusing nonlinearity [8–16]. Important structures that were investigated include the gap solitons [17] in optical lattices, multi-component solitons [18], vortices and multi-vortex configurations [19, 20], as well as solitonic vortices and vortex rings [21].

Typically, these structures are placed in simple confining potentials with the most canonical example being that of the parabolic trap [1–3]. However, this doesn't preclude the possibility that not only periodic [22], but also more elaborate non-harmonic potentials are accessible experimentally, as e.g. described in [23]. In fact, certain experimental techniques enable the formation of arbitrary trapping geometries [24] rendering atomic BECs a particularly well suited platform for exploring the interplay of nonlinearity and geometry. Nevertheless, other areas too, including nonlinear optics, provide case examples of different types of confinement through the manipulation of the optical medium's refractive index [25].

A particular motivation of the present work consists of a recent theoretical proposal towards exploring optical lattice settings with a torus topology in the context of BECs, with the atoms being confined to the surface of a torus [26]. This represents a striking example of a geometrically and topologically “nontrivial” trap which

bears great promise for novel nonlinear wave effects. Indeed there is a plethora of curved and confining surfaces of different geometry and topology that might be realizable and accessible experimentally using modern light manipulation techniques and tools. In parallel to that, there is an active interest in the field of pattern formation towards studying nonlinear partial differential equations on curved soft substrates; a prime example of that is the study of defect formation and localization through a generalized Swift-Hohenberg theory in elastic surface crystals [27, 28]. Motivated by an interweaving of these themes, our aim in the present work is to explore the existence, stability and dynamics of solitary waves in a nonlinear Schrödinger (NLS) model with attractive interparticle interactions on the surface of a torus. This is a prototypical *continuum Hamiltonian* case example as opposed to the lattice one of [26] and the dissipative dynamics of [27, 28] for the exploration of such dynamics.

Some of our main findings involve the identification of localized solutions in both angular directions of the torus. Such solutions come in two families, one on the inside and one on the outside of the torus. Also solutions depending on only one of the angular variables (independent of the other) are equally considered and their families have been identified. Among the doubly localized solutions, we find two varieties, one that is more solitonic in nature and one that is more reminiscent of a periodic solution that does not decay to the proximity of zero within its spatial variation. This last family, when centered on the outside of the torus is the only that is found to be spectrally stable sufficiently close to the small amplitude, i.e. near linear limit. The dynamics of localized solutions often lead to collapsing spots on the torus, while those depending on a single angle may lead to multiple such collapsing spots.

Our presentation is structured as follows. In section II

we provide the model, the benchmarks used for the linear problem and the theoretical setup of the nonlinear problem. Then, in section III, we will examine the different types of nonlinear solutions, localized and homogeneous ones, that we have identified in this geometric setting involving the Laplacian operator on the 2d torus. The continuation of the different branches of solutions versus the eigenvalue parameter μ which is the frequency of the solution, is given and the stability of these states is considered. When the solutions are identified as unstable their dynamics will be followed. Importantly, however, we also identify stable solutions sufficiently close to the linear limit of the problem. Lastly, we will summarize our findings in section IV and present a few of the many directions that are opening up for this promising research theme.

II. MODEL AND THEORETICAL SETUP

The torus with major radius R and minor radius r is centered at the origin and has parameterization in \mathbb{R}^3 given by $x = (R + r \cos(\theta)) \cos(\phi)$, $y = (R + r \cos(\theta)) \sin(\phi)$, and $z = r \sin(\theta)$. The toroidal angle is denoted by ϕ and poloidal angle θ . For a diagram of the torus and relevant parameters see Figure 1. Consider the 2D NLS equation on the surface of the torus with radii $R > r$ as follows

$$i\psi_t = -\frac{1}{2}\Delta\psi + V(\theta, \phi)\psi - \sigma|\psi|^2\psi \quad (1)$$

where $\sigma = 1$ is the focusing and $\sigma = -1$ the defocusing case. We will focus on the former setting in the present study. The Laplacian operator takes the form:

$$\Delta = \frac{1}{r^2}\partial_{\theta\theta} - \frac{\sin\theta}{r(R + r \cos\theta)}\partial_{\theta} + \frac{1}{(R + r \cos\theta)^2}\partial_{\phi\phi}. \quad (2)$$

In what follows, we define $\alpha = r/R$; moreover, as a starting point we will hereafter set $V(\theta, \phi) = 0$ to examine the potential of the torus for intrinsically localized states. A natural benchmark that we have performed en route to the consideration of the nonlinear problem has been the study of the linear spectrum of the underlying Laplacian operator as identified, e.g., in [29]. This spectral analysis has been done as a function of the parameter α characterizing the nature of the torus as regards the size of the minor radius r over the major radius R . A key feature in this case is that the relevant spectrum is discrete and consists of isolated eigenvalues due to the presence of a finite interval for the values of θ and ϕ (both running in the $[0, 2\pi]$ interval).

As is customary in the NLS setting, we consider stationary solutions by setting $\psi = e^{-i\mu t}u$ and obtaining the boundary value problem naturally with periodic boundary conditions

$$-\frac{1}{2}\Delta u + V(\theta, \phi)u - \sigma|u|^2u - \mu u = 0. \quad (3)$$

Once the solutions (among them we are interested in the ones that bear some form of localization) to Eq. (3) have been identified, their spectral stability can be monitored by setting

$$\psi = (u + \delta [a(\theta, \phi)e^{\nu t} + b(\theta, \phi)^*e^{\nu^* t}])e^{-i\mu t}. \quad (4)$$

From this, we obtain to order δ the linear system

$$\begin{bmatrix} M_1 & M_2 \\ -M_2^* & -M_1^* \end{bmatrix} \begin{bmatrix} a \\ b \end{bmatrix} = -i\nu \begin{bmatrix} a \\ b \end{bmatrix} \quad (5)$$

where $M_1 = \frac{1}{2}\Delta - V + \mu + 2\sigma|u|^2$ and $M_2 = \sigma u^2$. From Eq. (4) it follows that $\max(\text{Re}(\nu)) > 0$ corresponds to instability.

We focus primarily on the stationary solutions with some kind of localization. Such solutions are found to have the largest bulk of the waveform located either on the inside or the outside of the torus. These special locations on the torus correspond to where $\sin(\theta) = 0$. Next we separate categories of solutions based on whether the bulk of the solutions is centered near $\theta \approx 0$ on the outside of the torus (Types -out) or $\theta \approx \pi$ on the inside of the torus (Types -in). Note also that the operator in (2) remains translationally invariant in ϕ and so correspondingly we find some solutions which appear as a solid stripe wrapping around the torus in the toroidal ϕ direction.

The classification of solutions below is also based on which directions the solutions are localized. Using Newton's method to solve the stationary equation (3), one can select an initial guess bearing the desired localization properties of an intended solution in order to obtain convergence of the iterative process. We focus on solutions which have a single concentration of mass. All of the solutions which we have identified for the nonlinear problem with $\sigma = 1$ in the context of the present study lie on a spectrum between the category types outlined below, and have been obtained via continuation in the frequency parameter μ .

A Type I solution has localization properties similar to an initial guess in the form of

$$u = A_0 \text{sech} \left(\sqrt{|\mu|} [B_0(\theta - \theta_0)^2 + C_0(\phi - \phi_0)^2] \right) \quad (6)$$

for constants $A_0, B_0, C_0 \in \mathbb{R}$. For sufficiently large $|\mu|$ the solutions are localized both in the toroidal and in the poloidal direction. As $|\mu|$ transitions to smaller values the solution footprint grows and comes to wrap around the torus in both directions.

Such solutions appear as a two-dimensional sech-shape in both the θ and ϕ directions on the surface of the torus. There are two primary subtypes. We will call a Type I solution Type I-in if its bulk is on the interior of the torus; such solutions can be obtained from an initial guess of the form (6) with $\phi_0, \theta_0 \approx \pi$. Type I-out solutions bear mass predominantly on the exterior of the torus and they can be obtained from an initial guess (6) with $\phi_0 \approx 0$,

$\theta_0 \approx 0$. One of these configurations will correspond to a local energy minimum, while the other will correspond to a nonlinear Hamiltonian energy maximum though which one is which also depends on the value of α .

Type II solutions have localization properties similar to either an initial guess of the form

$$u = \text{sech}(A_0(\phi - \phi_0))(1 + B_0 \cos(\theta - \theta_0)) \quad (7)$$

for constants $A_0, B_0 \in \mathbb{R}$, or the same format but with θ, ϕ switched. These solutions are localized in the one direction and wrap around the torus (but without approaching zero) in the other direction. There are once again two sub-types. Type II-in solutions bear most of their mass on the interior of the torus and can be obtained from initial guess (7) with $\theta_0, \phi_0 \approx \pi$, and Type II-out solutions are principally localized on the exterior of the torus and can be obtained from initial guess (7) with $\theta_0 \approx 0, \phi_0 \approx \pi$. Recall, however, that type I and type II solutions can equivalently be localized at any other value of ϕ_0 , given the translational invariance of the Laplacian operator on ϕ .

Finally, Type III solutions have localization properties similar to an initial guess of the form

$$u = \text{sech}(A_0(\theta - \theta_0)) \quad (8)$$

for $A_0 \in \mathbb{R}$ a constant. Such resulting solutions appear as a localized shape in the poloidal θ direction and a solid stripe, i.e. it does not depend on and is thus uniform in the toroidal ϕ direction. The Type III-in solutions are approximately centered at $\theta_0 \approx \pi$ and the Type III-out at $\theta_0 \approx 0$.

As a diagnostic computed when constructing the bifurcation diagrams of the different states, we use the power of stationary solutions in the form of the following surface integral on the torus:

$$P = \int_0^{2\pi} \int_0^{2\pi} |\psi|^2 dS \quad (9)$$

where the surface element on the torus is $dS = |\hat{\phi} \times \hat{\theta}| d\theta d\phi$. Here hats denote the unit vectors in the different (toroidal and poloidal) directions. Thus, $|\hat{\phi} \times \hat{\theta}| = R + r \cos(\theta)$. Figures 2-7 show examples of stationary solutions with their magnitude shown in color on the surface of the corresponding torus. The power (used as a bifurcation parameter for the solution branch) and the maximum real part of the eigenvalues, identifying the spectral stability of the solution, are shown as a function of μ . Figure 8 shows examples of stationary solutions with the magnitude of solutions shown in terms of θ versus ϕ in the two-dimensional flat rectangle $[0, 2\pi] \times [0, 2\pi]$. Figures 9-11 show the dynamics of unstable solutions. These results will be discussed in more detail in the next section.

It is relevant to note that additional wave solutions of Eq. (3) exist and they can be found using an initial guess of $e^{il\phi}$ for $l = 1, 2, \dots$. Such solutions are unstable with

the fundamental (non-vortical) states of $l = 0$ being more dynamically robust than those with $l \neq 0$ for the cases we have considered. All examples observed for $l \neq 0$ feature blowup similar to the fate of the localized solutions described in the next section.

III. NUMERICAL RESULTS

We now turn to the presentation of our numerical findings. We will consider different values of α progressing from smaller to larger ones. In Figures 2 and 3 two branches of solutions are shown for $\alpha = 0.15$. One branch (solid line in Figure 2 (a)-(b)) has Type II-in solutions that are shown in Figure 2 (c)-(f). These solutions are sech-shaped in the toroidal direction and wrap around in the poloidal direction (without getting close to zero), with the bulk of the solution located on the interior of the torus. For larger values of $|\mu|$ the solutions have a smaller footprint on the torus, i.e. they become more localized as we expect in this setting of stronger non-linearity. For smaller values of $|\mu|$ on this branch the solution footprint is broader on the torus. This branch has increasing power until $\mu \approx -3.5$ where the branch has a turning point and continues to higher power as μ -values decrease (increase in absolute value). The other branch (dashed line) has Type II-out solutions that are shown on the torus in Figure 3 (a)-(d). These solutions are similar functionally but with the bulk of the solution located on the exterior of the torus. This branch has increasing and then decreasing power as a function of μ . This change in the power's monotonicity is caused by a change in the number of real eigenvalues, i.e., a change in stability. There are six real eigenvalues for higher values of $|\mu|$. Four are zero, and two have symmetric nonzero real values accounting for the instability of the branch. Around $\mu \approx -2.75$ the count of real eigenvalues changes to four (all are zero) and the solutions spectrally stabilize as the previously mentioned two nonzero real eigenvalues now merge onto the imaginary axis.

In Figures 4-5 four branches of solutions are demonstrated with $\alpha = 0.5$. One branch (solid line in Figure 4 (a)-(b)) has Type I-in solutions which are sech shaped in both directions. Here too, lower $|\mu|$ leads to a wider footprint, while higher $|\mu|$ has smaller footprint on the surface of the torus. The latter also leads to higher intensity in this more highly nonlinear regime. The Type I solutions are shown in Figure 4 (c)-(f). Another branch (dashed line) has Type I-out solutions which are localized in both directions for higher $|\mu|$ values, and when they are continued in the μ parameter to lower $|\mu|$ values they widen and eventually wrap around in the poloidal direction to approach Type II-out solutions. Other branches (dotted and dash-dotted line) are found here for $\alpha = 0.5$ in which solutions are of Type III-in and III-out as a solid stripe around the interior or exterior of the torus respectively. Generally these Type III branches are found to exist for other values such as $\alpha \gtrsim 0.45$ too. These branches

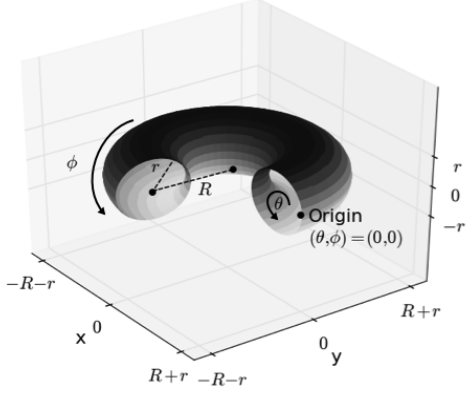


FIG. 1: Sketch of a torus with outer radius R and inner radius $r < R$. The arrows point in the direction of increasing toroidal angle ϕ and increasing poloidal angle θ .

typically carry larger mass, as the solitary structure is quasi-one-dimensional being uniform along the toroidal direction. The Types II and III examples are shown in Figure 5 (a)-(d).

In Figures 6-7 again four branches are found to exist for $\alpha = 0.75$. One branch (solid line in Figure 6 (a)-(b)) has Type I-in solutions which are sech-shaped in both directions for large $|\mu|$. As $|\mu|$ decreases, the solution widens and wraps around in the toroidal direction. This effectively implies that Type I solutions morph (for this value of α) into Type II solutions, upon the relevant variation of μ . This is to be contrasted with the $\alpha = 0.5$ (thinner torus) case described above where the solutions come to wrap around in both directions as $|\mu|$ decreases. For the $\alpha = 0.75$ case (fatter torus) the broadening of the solutions occurs only in the toroidal ϕ direction. Another branch (dashed line) is similar to the dashed line for the $\alpha = 0.5$ case described above where Type I-out solutions transition to Type II-out solutions by widening and wrapping around in the poloidal direction. See Types I and II solution shown in Figure 6 (c)-(f) and in Figure 7 (c)-(d). The third and fourth branches which are of Type III solutions shown in Figure 7 (a)-(b) are similar to the $\alpha = 0.5$ case and they exist for other values of $\alpha \gtrsim 0.45$. It is relevant to note in passing that all of these solutions for the larger values of α have been found to be unstable.

In Figure 8 the magnitude of some solutions is shown in a flat rendering on the rectangle $[0, 2\pi] \times [0, 2\pi]$ with respect to θ and ϕ to give a “planar” sense of the waveforms. The top row (a)-(b) shows typical Type II solutions which wrap around in the toroidal direction (without returning to the proximity of zero) and are localized in the poloidal direction. The middle row (c)-(d) shows a standard example of a Type I solutions localized in both directions for sufficiently large values of $|\mu|$. Upon para-

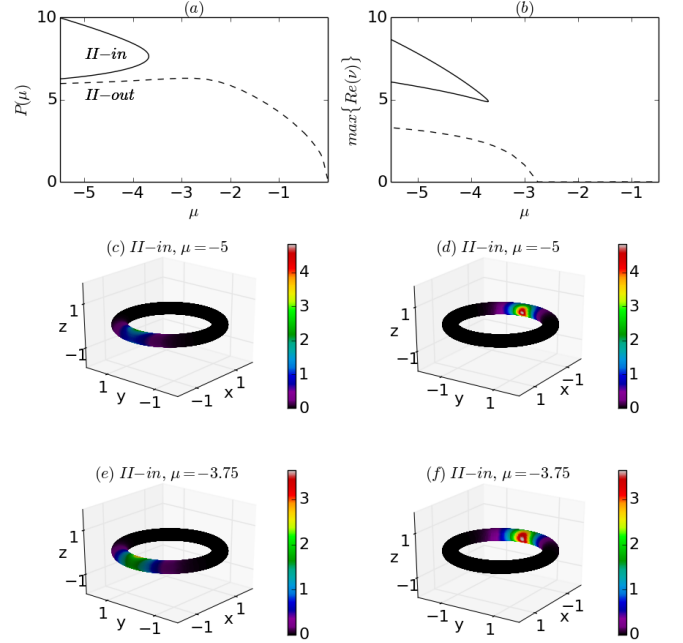


FIG. 2: These graphs correspond to $\alpha = 0.15$ and $R = 1.6$ so that $r = \alpha R = 0.24$. In (a) the power $P(\mu)$ of solutions is shown as a function of μ . In (b) the maximum real part of the eigenvalues ν is shown as a function of μ . The magnitude of stationary solutions $|u|$ is shown according to the colorbar on the surface of the torus. A solution with $\mu = -5$ in subfigures (c) and (d) (two views, front and back) is of Type II-in, and although the mass of the solution is principally located on the interior of the torus a small amplitude does wrap around in the poloidal direction. A continuation of this solution in the parameter μ gives the other Type II-in solution with $\mu = -3.75$ in subfigures (e) and (f) (two views, front and back) that is localized in the toroidal direction and wraps around in the poloidal direction. As the branch continues the power curve turns upwards to greater power values the solutions continue to broaden in the toroidal direction. The power and eigenvalues for these solutions and others obtained by continuation in μ are shown in the top panels with a solid line. Examples of solutions in Figure 3 correspond to the other branch shown with a dashed line. The latter branch is spectrally stable if μ is sufficiently large (and its absolute value sufficiently small).

metric continuation in μ the solution footprint expands in both directions so that for small enough values of $|\mu|$ solutions wrap around in both toroidal and poloidal directions. The bottom row (c)-(f) shows some basic examples of Type III solutions which represent a solid stripe in the toroidal direction.

According to the panels (b) in Figures 2, 4, 6 which summarize the stability features of the obtained solutions, all the branches identified as having stable solutions for a range of frequencies are of Type II-out, i.e., they are localized in the toroidal direction but do not approach zero along the poloidal direction, and they have most of their mass on the outside of the torus. Notice

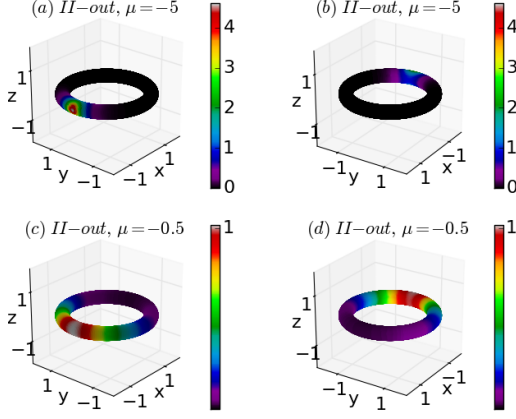


FIG. 3: These graphs on the torus are similar to those seen in Figure 2. The solutions here correspond to the power and eigenvalue curves from Figure 2 with a dashed line. The solution with $\mu = -5$ in subfigures (a) and (b) (front and back views) is of Type II-out, having its bulk on the exterior of the torus but also wrapping around in the poloidal direction. This solution originates from continuation in μ from the other solution of Type II-out in subfigures (c) and (d) (front and back views) which has value $\mu = -0.5$. The solution with $\mu = -5$ has more mass located on the exterior of the torus.

that this happens only for an interval of μ , indicating that this stability is a byproduct of the interplay between the nonlinearity and geometry. For the two-dimensional plane in the absence of curvature, recall that solitary wave two dimensional solutions are prone to collapse as is discussed in detail e.g. in [30, 31]. On the other hand, the geometry breaks the translational invariance of the model, as well as the scale invariance thereof, leading to the existence (for sufficiently strong nonlinearity) of real eigenvalue pairs. It is only for this (II-out) branch of solutions and for a range of frequencies in the vicinity of the small amplitude limit that the interplay of curvature and nonlinearity permits spectral stability. Such stable solutions exist for a wider range of μ -values if α is small (on a thinner torus), and they exist for a smaller range of μ -values for α large (on a fatter torus). Plots of stable solutions are shown in plots (c) and (d) in Figures 3, 5, 7 for $\alpha = 0.15, 0.5, 0.75$ respectively. By comparing these stable solutions one can see that the amount of mass of these stable solutions which wraps around in the poloidal direction starts to diminish as α increases.

It is relevant to note that from the stability perspective, solutions of Type I and Type II possess two pairs of eigenvalues at the origin, reflecting the invariance with respect to phase and the translational invariance along the toroidal ϕ direction. On the other hand, this freedom to locate the solution arbitrarily in ϕ is lost in the Type-III solutions leading to a single pair of eigenvalues at the origin of the spectral plane. In the case of the stable

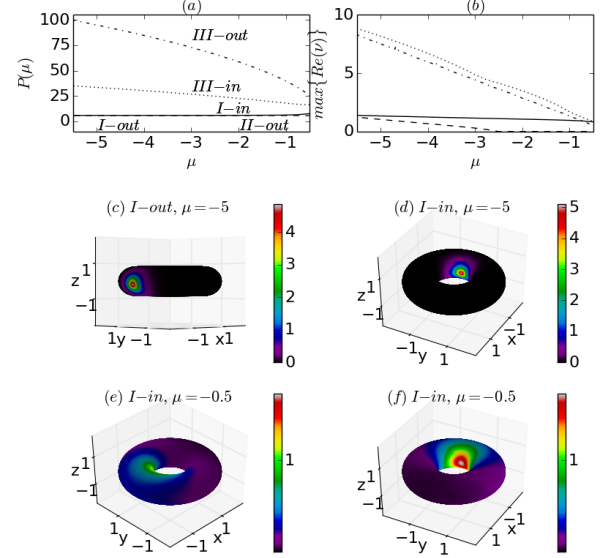


FIG. 4: As in Figure 2 but for the values $\alpha = 0.5$, $R = 1.6$, and $r = \alpha R = 0.8$. The solid lines in subfigures (a) and (b) correspond to Type I-in solutions which look as a sech shape in both directions. Examples on this branch are shown in (e) and (f) $\mu = -0.5$ (front and back views) and also in (d) for $\mu = -5$. The dashed lines in subfigures (a) and (b) correspond to Type I-out solutions which are sech shape on the exterior of the torus and after continuation to lower values of $|\mu|$ transition into Type II-out solutions which wrap around in the poloidal direction. In (c) an example is shown on the dashed branch for $\mu = -5$ which is sech shaped in both directions.

Type II-out solutions reported above, e.g., for $\alpha = 0.15$, there are two additional eigenvalue pairs on the imaginary axis indicating the spectral stability of the state (since real eigenvalues are absent in this case). Aside from this branch of the form of II-out, all other identified solutions have been found to be unstable. A natural subsequent question then is that of the dynamical evolution of these unstable solutions. After time propagation according to Eq. (1) the unstable solutions mostly experience blowup in the case examples that we have examined. Such blowup can occur either on the inside or on the outside of the torus. This is determined predominantly by the nature of the solution, but also from the nature of the associated perturbation.

Examples of blowup are shown in Figures 9-10. In some cases a Type I-in or Type II-in unstable solution may approach one of the Type II-out stable solutions described above. An example is shown in Figure 11. Such a phenomenology is the only alternative to collapsing behavior that we have observed in the torus dynamics case examples that we have considered.

Lastly, we briefly consider the possibility of vortical so-

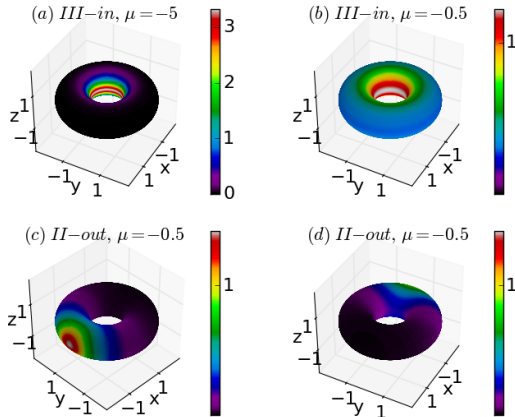


FIG. 5: These graphs on the torus are similar to those provided in Figure 4. The solutions subfigures (a) and (b) are of Type III-in and correspond to the dotted line branch from Figure 4. For these Type III-in solutions the stripe visible on the interior of the torus is solid around the hole of the torus due to the independence of the solution on ϕ . The solution shown here in (c) and (d) (front and back views) is a Type II-out example with $\mu = -0.5$ wrapping around in the poloidal direction. This lies on the dashed branch from Figure 4.

lutions bearing an additional phase factor of $e^{il\phi}$. An example of this type for the waveform of Type III is shown in Figure 12. From the left panels illustrating the spectral planes (ν_r, ν_i) of eigenvalues $\nu = \nu_r + i\nu_i$, we can infer that solutions with $l = 1$ are more unstable (via a larger number of unstable modes and associated growth rates) than the $l = 0$ ones. This has been typical in the cases we have examined herein, hence we do not focus on these vortical waveforms further.

IV. CONCLUSIONS AND OUTLOOK

In the present work, we have set the stage for considering nonlinear Schrödinger equations and related dispersive wave models on the torus. While in the mathematical community, this is synonymous to a periodic boundary condition system, as opposed to an infinite domain, here the details of the geometry critically affect the linear (Laplacian) operator adding a natural parameter to this system, namely the ratio of minor over major axis of the torus. Furthermore, the explicit presence of the poloidal variable and the finite size periodicity of the toroidal one induce drastic differences from the translationally invariant two-dimensional case that is familiar in the NLS realm [30, 31]. Here, we encounter a situation where (partially) translational as well as scale invariance are broken by the presence of curvature leading to a potential spectral destabilization of the resulting solutions. We have identified different types of states including ones

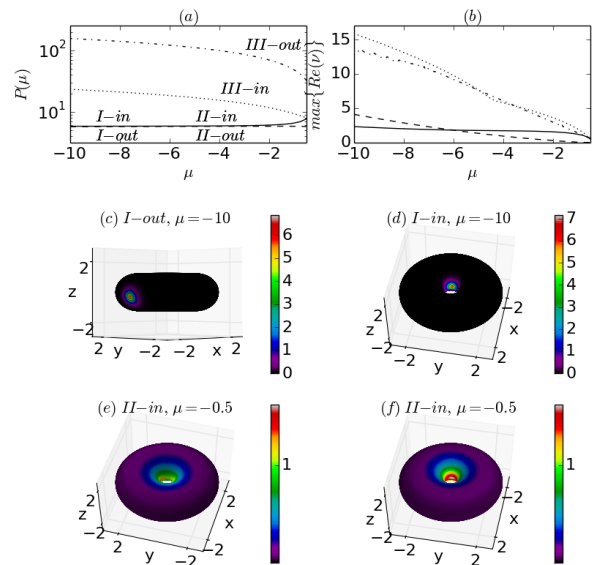


FIG. 6: These graphs are similar to Figure 2 but here with values $\alpha = 0.75$, $R = 1.6$, and $r = \alpha R = 1.2$. Since the power becomes large for some branches in (a), this graph is displayed with a log scale on the y-axis. The solid lines in (a) and (b) correspond to localized in both directions Type I-in solutions for higher $|\mu|$ values which upon continuation to lower $|\mu|$ values give Type II-in solutions as they widen in the toroidal direction. Examples on this solid line branch are seen in subfigures (e) and (f) for $\mu = -0.5$ (front and back views) and also in (d) for $\mu = -10$. The dashed lines in (a) and (b) correspond to Type I-out solutions for higher values of $|\mu|$ which transition into Type II-out solutions for lower values of $|\mu|$. In (c) an example is shown on this dashed branch for $\mu = -10$.

that are localized in both spatial directions, localized in one and wrapping around (yet staying far from zero) in the other, as well as localized in one and homogeneous in the other. Among these, we found that only the second type can have a range of frequencies (near the linear limit) where the solutions are spectrally stable. For too high frequencies and for all branches, nonlinearity takes over and leads to collapse instabilities. However, sufficiently close to the small amplitude limit, the interplay of curvature and nonlinearity may dynamically lead to periodic oscillations around a spectrally stable state, as shown in our dynamics above.

Naturally, we feel that this first stab at this class of problems opens numerous new directions to consider. A very canonical one among them is to explore the possibility of self-defocusing nonlinearities. On the one hand, these are canonical for numerous atomic gases such as ^{87}Rb or ^{23}Na [1, 2] while on the other hand, they present the potential for fundamentally distinct structures including ones bearing vorticity in the two-dimensional

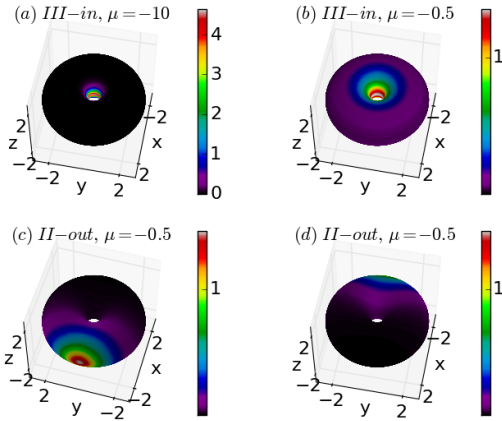


FIG. 7: These graphs on the torus are similar to those seen in Figure 6. The solutions in (a) and (b) are of Type III-in and correspond to the dotted line branch from Figure 6. For these Type III-in solutions the stripe visible on the interior of the torus is solid around the hole of the torus given the homogeneous nature of the solution in the corresponding (ϕ) variable. The solution here in subfigures (c) and (d) (front and back views) is a Type II-out example with $\mu = -0.5$ which lies on the dashed branch from Figure 6 and it wraps around in the poloidal direction.

realm. This vorticity could be in the form of localized vorticity (point vortices), or in that of vorticity filaments, such as rings wrapping potentially around either the toroidal or the poloidal direction. Exploring such states and their stability has been a major theme in atomic BECs [3] and its interplay with geometry in this setting would present novel challenges and potential outcomes. Yet another relevant possibility could be to remain on the focusing interaction realm but “negate” the possibility of collapse by introducing photorefractive nonlinearities as, e.g., in [32]. In this case, the model at sufficiently high intensity returns to its linear form and therefore collapse type instabilities no longer occur. It would be especially relevant in this latter setting to explore which among the different types of unstable solutions identified herein become stabilized (or possibly vice versa). These studies will be deferred to future work.

Acknowledgements. J.D.A. gratefully acknowledges computing support based on the Army Research Office ARO-DURIP Grant W911NF-15-1-0403.

-
- [1] L. P. Pitaevskii and S. Stringari, *Bose-Einstein Condensation and Superfluidity*, Oxford University Press (Oxford, 2016).
 - [2] C.J. Pethick and H. Smith, *Bose-Einstein condensation in dilute gases*, Cambridge University Press (Cambridge, 2002).
 - [3] P. G. Kevrekidis, D. J. Frantzeskakis and R. Carretero-González, *The Defocusing Nonlinear Schrödinger Equation*, SIAM (Philadelphia, 2015).
 - [4] L. Khaykovich, F. Schreck, G. Ferrari, T. Bourdel, J. Cubizolles, L.D. Carr, Y. Castin and C. Salomon, *Science* **296**, 1290 (2002).
 - [5] K. E. Strecker, G. B. Partridge, A. G. Truscott and R. G. Hulet, *Nature* **417**, 150 (2002).
 - [6] L. Khaykovich, F. Schreck, G. Ferrari, T. Bourdel, J. Cubizolles, L. D. Carr, Y. Castin and C. Salomon, *Science* **296**, 1290 (2002).
 - [7] S. L. Cornish, S. T. Thompson and C. E. Wieman, *Phys. Rev. Lett.* **96**, 170401 (2006).
 - [8] S. Burger, K. Bongs, S. Dettmer, W. Ertmer, K. Sengstock, A. Sampera, G.V. Slyapnikov and M. Lewenstein, *Phys. Rev. Lett.* **83**, 5198 (1999).
 - [9] J. Denschlag, J.E. Simsarian, D.L. Feder, Charles W. Clark, L.A. Collins, J. Cubizolles, L. Deng, E.W. Hangle, K. Helmerson, W.P. Reinhardt, S.L. Rolston, B.I. Schneider and W.D. Phillips, *Science* **287**, 97 (2000).
 - [10] C. Becker, S. Stellmer, P. Soltan-Panahi, S. Dörscher, M. Baumert, E.-M. Richter, J. Kronjäger, K. Bongs and K. Sengstock, *Nature Phys.*, **4**, 496 (2008).
 - [11] A. Weller, J. P. Ronzheimer, C. Gross, J. Esteve, M. K. Oberthaler, D. J. Frantzeskakis, G. Theoharis and P. G. Kevrekidis, *Phys. Rev. Lett.* **101**, 130401 (2008).
 - [12] P. Engels and C. Atherton, *Phys. Rev. Lett.* **99**, 160405 (2007).
 - [13] S. Stellmer, C. Becker, P. Soltan-Panahi, E.-M. Richter, S. Dörscher, M. Baumert, J. Kronjäger, K. Bongs and K. Sengstock, *Phys. Rev. Lett.* **101**, 120406 (2008).
 - [14] G. Theoharis, A. Weller, J. P. Ronzheimer, C. Gross, M. K. Oberthaler, P. G. Kevrekidis and D. J. Frantzeskakis, *Phys. Rev. A* **81**, 063604 (2010).
 - [15] I. Shomroni, E. Lahoud, S. Levy and J. Steinhauer, *Nat. Phys.* **5**, 193 (2009).
 - [16] D. J. Frantzeskakis, *J. Phys. A* **43**, 213001 (2010).
 - [17] O. Morsch and M. Oberthaler, *Rev. Mod. Phys.* **78**, 179 (2006).
 - [18] P.G. Kevrekidis and D.J. Frantzeskakis, *Rev. Phys.* **1**, 140 (2016).
 - [19] A. L. Fetter and A.A. Svidzinsky, *J. Phys.: Cond. Mat.* **13**, R135 (2001).
 - [20] A. L. Fetter, *Rev. Mod. Phys.* **81**, 647 (2009).
 - [21] S. Komineas, *Eur. Phys. J.- Spec. Topics* **147**, 133 (2007).
 - [22] O. Morsch and M. K. Oberthaler, *Rev. Mod. Phys.* **78**, 179 (2006).
 - [23] H. Ott, J. Fortágh, S. Kraft, A. Günther, D. Komma and C. Zimmermann *Phys. Rev. Lett.* **91**, 040402 (2003).
 - [24] K. Henderson, C. Ryu, C. MacCormick and M.G. Boshier, *New J. Phys.* **11**, 043030 (2009).
 - [25] Yu.S. Kivshar and G.P. Agrawal, *Optical solitons: from fibers to photonic crystals*, Academic Press (San Diego, 2003).

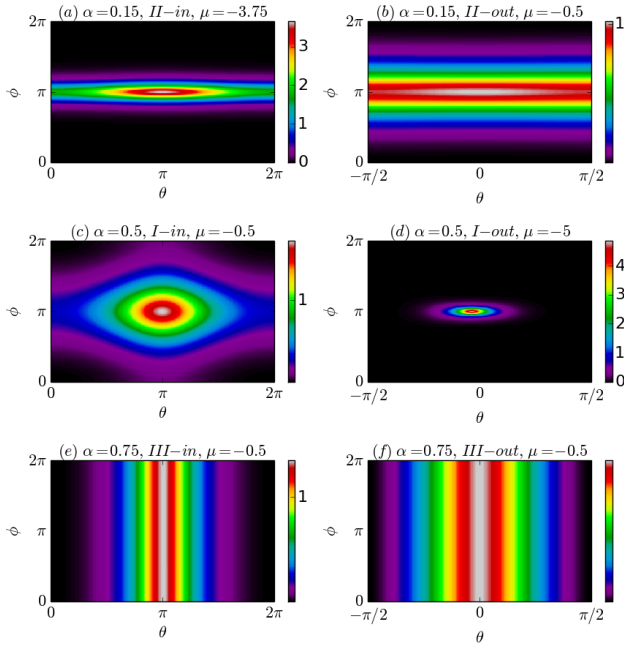


FIG. 8: The graphs demonstrate some of the different shapes of solutions, represented flat with respect to $\theta, \phi \in [0, 2\pi]$. Plot (a) here is the same solution as (f) in Figure 2. Subfigure (b) here is the same solution as (d) on Figure 3; since this is an out-type solution the flat axis here is centered at the peak of the solution. Subfigures (c) and (d) here are the same solutions in (f) and (c) in Figure 4 respectively. Subfigures (e) and (f) here are Type III-in and Type III-out respectively for $\alpha = 0.75$ at $\mu = -0.5$.

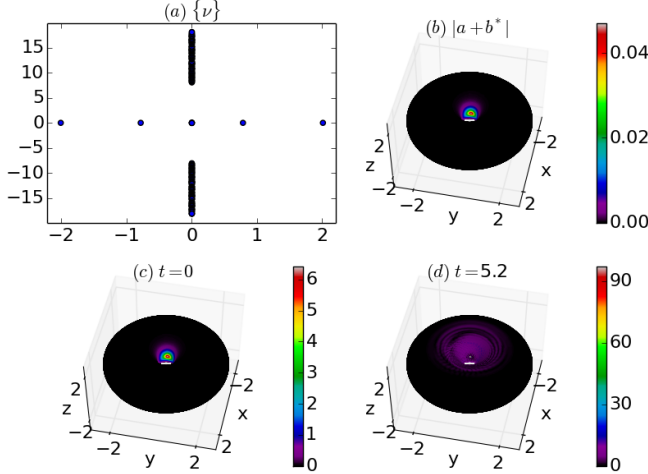


FIG. 9: For $\alpha = 0.75$, $R = 1.6$ and $\mu = -8$ the time propagation of a stationary solution is demonstrated. In (a) the eigenvalues $\{\nu\}$ are shown in the complex plane. In (b) the magnitude of $a + b^*$ is shown on the torus according to the colorbar values, where $[a, b]^T$ is the eigenvector corresponding to the eigenvalue with max real part. In (c)-(d) the stationary solution is shown at $t = 0$ and at a later time $t = 5.2$ when the solution approaches blowup.

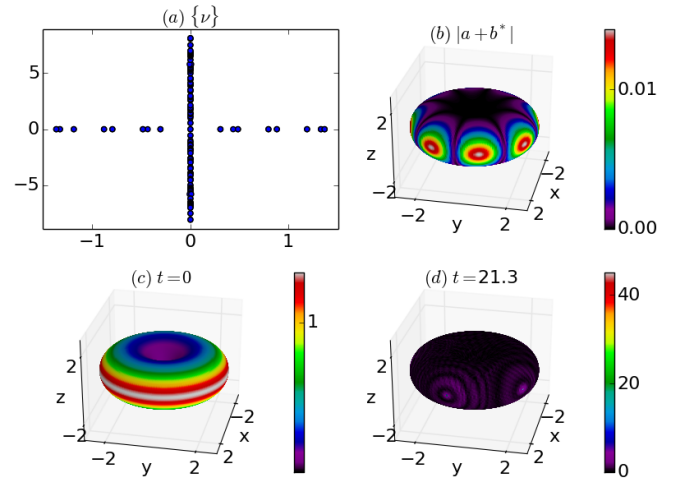


FIG. 10: As in Figure 9 but for the values $\alpha = 0.75$, $R = 1.6$ and $\mu = -1$. The stationary solution is shown at $t = 0$ and at a later time $t = 21.3$ when the solution approaches blowup at multiple spots around the exterior of the torus.

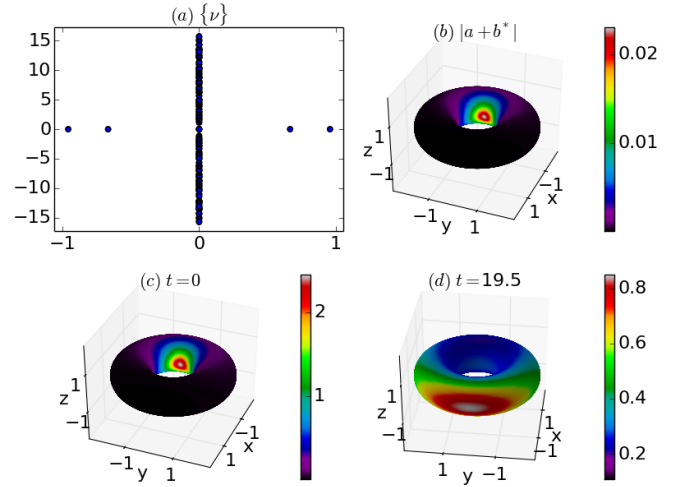


FIG. 11: As in Figure 9 but for the values $\alpha = 0.5$, $R = 1.6$ and $\mu = -1$. The stationary solution is shown at $t = 0$ and at a later time $t = 19.4$ when the solution mass moves to the exterior of the torus. In this example a Type I-in solution approaches a Type II-out solution rather than being led to collapse as a result of its instability.

- [26] H. Kim, G. Zhu, J.V. Porto and M. Hafezi Phys. Rev. Lett. **121**, 133002 (2018).
- [27] F. López Jiménez, N. Stoop, R. Lagrange, J. Dunkel and P.M. Reis Phys. Rev. Lett. **116**, 104301 (2016).
- [28] N. Stoop, R. Lagrange, D. Terwagne, P.M. Reis and J. Dunkel, Nat. Materials **14**, 337 (2015).
- [29] R. Glowinski and D.C. Sorensen, in *Partial Differential Equations: Modeling and Numerical Simulation*, R. Glowinski and P. Neittaanmäki (Eds), Springer-Verlag (Berlin, 2008) p. 225.
- [30] C. Sulem and P.L. Sulem, *The Nonlinear Schrödinger Equation*, Springer-Verlag (New York, 1999).

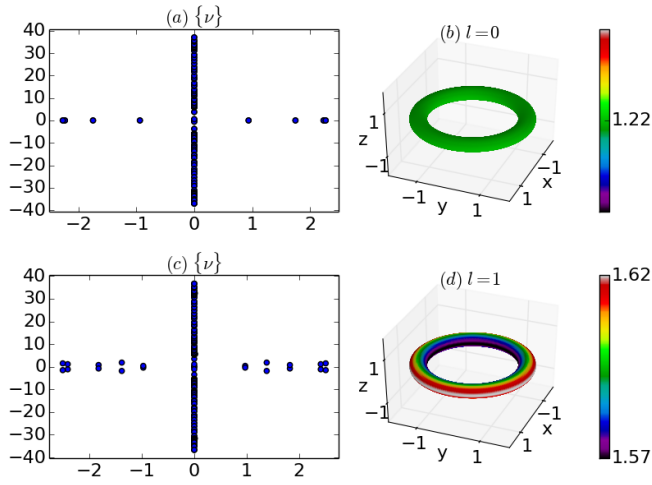


FIG. 12: Plot (a) shows the eigenvalues of the solution for $l = 0$ which is shown on the torus in (b). Plot (c) similarly for $l = 1$ in (d). Both examples correspond to $\alpha = 0.15$ and $\mu = -2.36$.

- [31] G. Fibich, *The Nonlinear Schrödinger Equation*, Springer-Verlag (Heidelberg, 2015).
 [32] J. Yang, New J. Phys. **6**, 47 (2004).